Journal of Asian Earth Sciences 96 (2014) 353–360

Contents lists available at ScienceDirect

Journal of Asian Earth Sciences

journal homepage: www.elsevier.com/locate/jseaes

Geological variation in *S*-wave velocity structures in Northern Taiwan and implications for seismic hazards based on ambient noise analysis

Ya-Chuan Lai [a,*], Bor-Shouh Huang [a], Yu-Chih Huang [a,b], Huajian Yao [c], Ruey-Der Hwang [d], Yi-Ling Huang [e], Wen-Yen Chang [f]

[a] Institute of Earth Sciences, Academia Sinica, Taipei, Taiwan
[b] Taiwan Volcano Observatory at Tatun, Ministry of Science and Technology, Taipei, Taiwan
[c] Laboratory of Seismology and Physics of Earth's Interior, School of Earth and Space Sciences, University of Science and Technology of China, Hefei, Anhui, China
[d] Department of Geology, Chinese Culture University, Taipei, Taiwan
[e] Institute of Applied Geosciences, National Taiwan Ocean University, Keelung, Taiwan
[f] Department of Natural Resources and Environmental Studies, National Dong Hwa University, Hualien, Taiwan

ARTICLE INFO

Article history:
Received 21 March 2014
Received in revised form 20 August 2014
Accepted 29 August 2014
Available online 17 September 2014

Keywords:
Ambient noise
Empirical Green's function (EGF)
Rayleigh wave
Group velocity

ABSTRACT

Ambient noise analysis in Northern Taiwan revealed obvious lateral variations related to major geological units. The empirical Green's functions extracted from interstation ambient noise were regarded as Rayleigh waves, from which we analyzed the group velocities for period from 3 to 6 s. According to geological features, we divided Northern Taiwan into seven subregions, for which regionalized group velocities were derived by using the pure-path method. On average, the group velocities in mountain areas were higher than those in the plain areas. We subsequently inverted the *S*-wave velocity structure for each subregion down to 6 km in depth. Following the analysis, we proposed the first models of geology-dependent shallow *S*-wave structures in Northern Taiwan. Overall, the velocity increased substantially from west to east; specifically, the mountain areas, composed of metamorphic rocks, exhibited higher velocities than did the coastal plain and basin, which consist of soft sediment. At a shallow depth, the Western Coastal Plain, Taipei Basin, and Ilan Plain displayed a larger velocity gradient than did other regions. At the top 3 km of the model, the average velocity gradient was 0.39 km/s per km for the Western Coastal Plain and 0.15 km/s per km for the Central Range. These *S*-wave velocity models with large velocity gradients caused the seismic waves to become trapped easily in strata and, thus, the ground motion was amplified. The regionalized *S*-wave velocity models derived from ambient noises can provide useful information regarding seismic wave propagation and for assessing seismic hazards in Northern Taiwan.

1. Introduction

Taiwan is an active tectonic region, where the orogeny is created by the convergence between the Eurasian plate and the Philippine Sea plate. In Northern Taiwan, the Philippine Sea plate subducts northward to create complex tectonics and geological features (Fig. 1), as validated according to seismicity (Tsai, 1986; Wang and Shin, 1998) and seismic tomography (cf. Kim et al., 2005; Wu et al., 2007b; Kuo-Chen et al., 2012). In Taiwan, plate convergence strongly controls principle geological structures, resulting in a northeastward tendency. The primary units from west to east are the Western Coastal Plain, Western Foothills, Hsueshan Range, Central Range, and Coastal Range (Ho, 1986). In addition, the Tatun Volcano Group and the Taipei Basin in Northern Taiwan are the crucial local geological structures.

P-wave tomography is an efficient method for examining the features of plate tectonics (Kim et al., 2005; Wu et al., 2007b; Kuo-Chen et al., 2012). However, the resolution for regional seismic tomography is limited by the geometric configuration between the earthquake locations and seismic stations; specifically, the depth resolutions of regional seismic tomography in the mantle and a few kilometers of shallow structures are also low. Regarding seismic hazard assessment, the underground structures are crucial for predicting the ground motion in an actively seismicity region, particularly for the shallow *S*-wave velocity structures near the surface. Consequently, conducting *S*-wave tomography is quite important but difficult, because of its inexact picking in the *S*-wave arrival. Regional short-period surface waves (Chung and Shin, 1999; Hwang et al., 2003) and microtremor array analyses have typically

* Corresponding author.
E-mail address: yachuan@earth.sinica.edu.tw (Y.-C. Lai).

http://dx.doi.org/10.1016/j.jseaes.2014.08.039
1367-9120/

been used to investigate shallow *S*-wave structures (Satoh et al., 2001; Huang and Wu, 2006; Lin et al., 2009; Wu and Huang, 2013). However, the spatial resolution for regional short-period surface waves and microtremor array analyses is too low for acquiring a dense and uniform ray-path distribution. To enhance the spatial resolution, interstation short-period surface waves (i.e., empirical Green's function, EGF) are extracted from the ambient noise and have served as a helpful tool for exploring shallow *S*-wave structures in the past decade (Shapiro and Campillo, 2004; Sabra et al., 2005; Shapiro et al., 2005; Yao et al., 2006). Recent studies have shown that ambient noise not only increases the spatial resolution but also improves the retrieval of short-period surface waves down to a few seconds (cf. Huang et al., 2010, 2012; You et al., 2010). Early, the short-period group velocity map of Northern Taiwan developed previously by You et al. (2010) indicated a high consistency between the velocity variation and geological units. Here, we did not make tomography, but regionalizing Northern Taiwan on the basis of the major geological units to illustrate the average group velocity and its corresponding *S*-wave structure.

In 2008–2009, the TAiwan Integrated GEodynamic Research (TAIGER) project, which is focused on investigating plate tectonics in Taiwan, has established numerous seismic stations throughout Taiwan (cf. Wu et al., 2007a, 2014; Okaya et al., 2009). The data collected through the TAIGER project provide an excellent opportunity to examine shallow-depth *S*-wave structures by conducting an ambient noise analysis. In this study, we combined the stations from the TAIGER project and several permanent stations (Fig. 1), at which Rayleigh waves were captured from the vertical-component recordings, to complete the ambient noise analysis. We subsequently determined the interstation Rayleigh-wave group velocity and derived the regional group velocities based on the geological features in Northern Taiwan. Finally, the *S*-wave velocity structure of each geological unit was inverted. Such geology-based 1-D velocity structure would be useful for ground motion simulation to address the sensitivity of model parameters, such like low-velocity sediments, velocity contrast, and velocity gradient. Our work revealed the lateral variations in structures as well as the shallow *S*-wave velocity, facilitating ground-motion prediction and, thus, seismic hazard assessment. In addition, the regionalized models can also be applied to local earthquake location and constraint of regional tomography.

2. Data

In addition to seismic recordings acquired from two linear arrays of the TAIGER project (cf. Wu et al., 2007a, 2014; Okaya et al., 2009) and Broadband Array in Taiwan for Seismology (BATS), data from one temporary array in the Northern Taiwan area operated by the Institute of Earth Sciences (IES, Academia Sinica, Taiwan) were also included. A total of fifty-one broadband stations (Fig. 1) throughout Northern Taiwan were used to create good path coverage by station pairs. We collected vertical-component continuous recordings for three months, from February to April, 2008. Several procedures prior to the ambient noise analysis were conducted. First, we divided the continuous raw data into daily records and then visually checked the data quality. The daily ones that have large periodic impulse were thus removed. Second, after removing the instrumental response, the sampling rate of recording was changed to 1 Hz. Finally, the daily continuous seismic data was band-pass filtered between 3 and 20 s. To retrieve reasonable dispersion curves, the interstation distance must be three times larger than the longest wavelength (cf. Yao et al., 2006; Bensen et al., 2007). Therefore, we adopted only the station pairs with interstation distances exceeding 40 km.

3. Analysis and results

3.1. Empirical Green's function derived from ambient noise analysis

The empirical Green's function, EGF, of surface waves extracted from the time derivative of the ambient noise cross-correlation

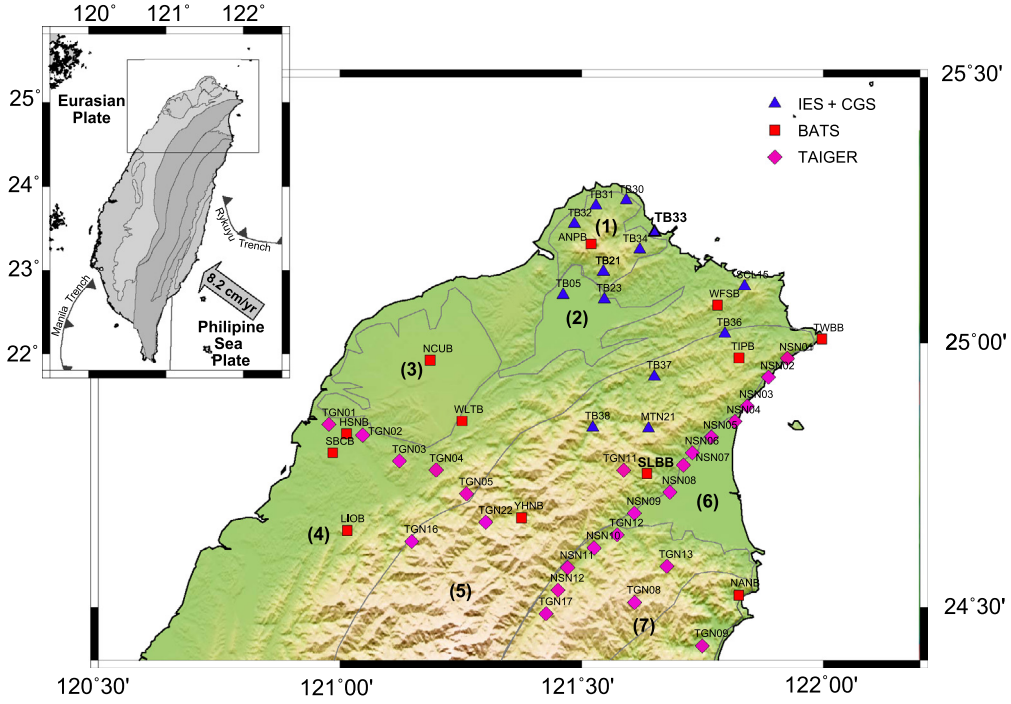

Fig. 1. The upper left diagram shows the tectonic setting of Taiwan. The rectangle marks the survey area. The broadband seismic stations used are marked by triangles (IES and CGS), squares (BATS), and diamonds (TAIGER). The major geologic units in Northern Taiwan are (1) Tatun Volcano Group, (2) Taipei Basin, (3) Western Coastal Plain, (4) Western Foothills, (5) Hsueshan Range, (6) Ilan Plain, and (7) Central Range.

function has been demonstrated by Lobkis and Weaver (2001) and extensively applied to seismology (Shapiro and Campillo, 2004; Sabra et al., 2005; Shapiro et al., 2005; Yao et al., 2006). The EGF, $\widehat{G}(t)$, can be expressed as follows.

$$\frac{dC_{AB}(t)}{dt} = -\widehat{G}_{AB}(t) + \widehat{G}_{BA}(-t) \approx -G_{AB}(t) + G_{BA}(-t) \quad (1)$$

where $C_{AB}(t)$ is the cross-correlation function between Stations A and B; G is the actual Green's function; $\widehat{G}_{AB}(t)$ represents the EGF at Receiver B for a fictitious source at Station A, and $\widehat{G}_{BA}(-t)$ is the time-reversed EGF at Receiver A for a fictitious source at Station B. Moreover, $\widehat{G}_{AB}(t)$ is only nonzero when $t \geqslant 0$, and $\widehat{G}_{BA}(-t)$ is only nonzero when $t \leqslant 0$. To reduce the influence of a large earthquake on the ambient noise analysis, we used the one-bit cross-correlation method, in which the signal amplitude is normalized to 1.0 for values greater than zero and to −1.0 for values lower than zero (Derode et al., 1999; Campillo and Paul, 2003). Fig. 2 shows the data processing executed to capture the EGF by using the station pair of SLBB-TB33 (also see Fig. 1).

For all available station pairs, we estimated each EGF for each interstation by using daily continuous data, and subsequently stacked the EGFs of three months to obtain the average EGF (aEGF) (Fig. 3). Considering the stability of each EGF, the cross-correlation coefficient between daily EGF and aEGF for each station pair was calculated to judge whether the daily EGF was available or not. Certain EGFs exhibited a low cross-correlation coefficient, which might be related to time and polarity problems (You et al., 2010). We adopted a daily EGF with a cross-correlation coefficient greater than 0.5 and thus renewed the aEGF for following velocity analysis. Fig. 4 shows an example of the station pair SLBB-TB33 to account for the choice of daily EGF. Spectrum shows that the energy of aEGFs was concentrated on the low-period band, particularly for periods ranging at 3–6 s, correlating with oceanic microseisms (Bromirski et al., 2005). In Fig. 3, the asymmetry of EGFs suggested that the source of noise was inhomogeneous and that noise propagated from coastal to inland areas, as addressed by Chen et al. (2011). After a detailed selection analysis of EGFs, we adopted 280 interstation EGFs (Fig. 5a) to determine their corresponding group velocities (Fig. 5b), which were further used to invert the *S*-wave velocity structures in Northern Taiwan.

3.2. Group velocity dispersions

The interstation EGFs, analyzed by the ambient noise, were on behalf of Rayleigh waves (cf. Shapiro and Campillo, 2004). Previous studies have calculated the group velocity (Sabra et al., 2005; Huang et al., 2012) or phase velocity (Yao et al., 2006; Huang et al., 2010) by using the extracted Rayleigh waves to investigate the velocity variations. However, to avoid an ambiguous calculation of phase velocity attributable to the 2π-phase problem (Yao et al., 2006), we determined the group velocity of a Rayleigh wave by using the Multiple Filter Technique (Dziewonski et al., 1969;

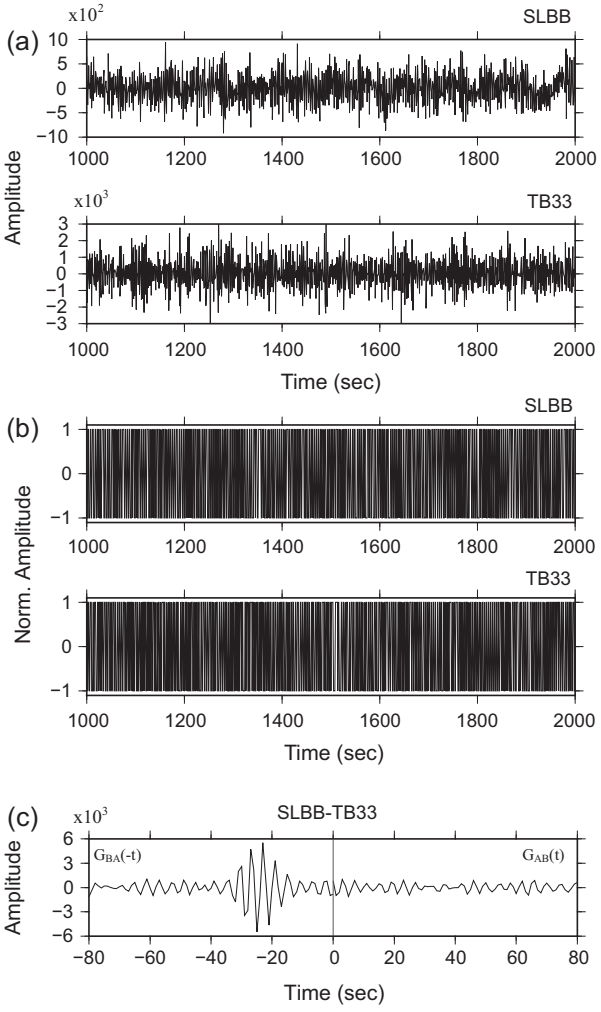

Fig. 2. An example of ambient noise analysis using one-bit cross-correlation at the station pair of SLBB-TB33. (a) Raw data filtered between 3 and 20 s. (b) One-bit normalized data from (a). (c) The daily EGF for periods of 3–20 s was extracted from the time derivative of the one-bit cross-correlation function. The EGF shows obvious asymmetry, indicating noise propagation from TB33 to SLBB.

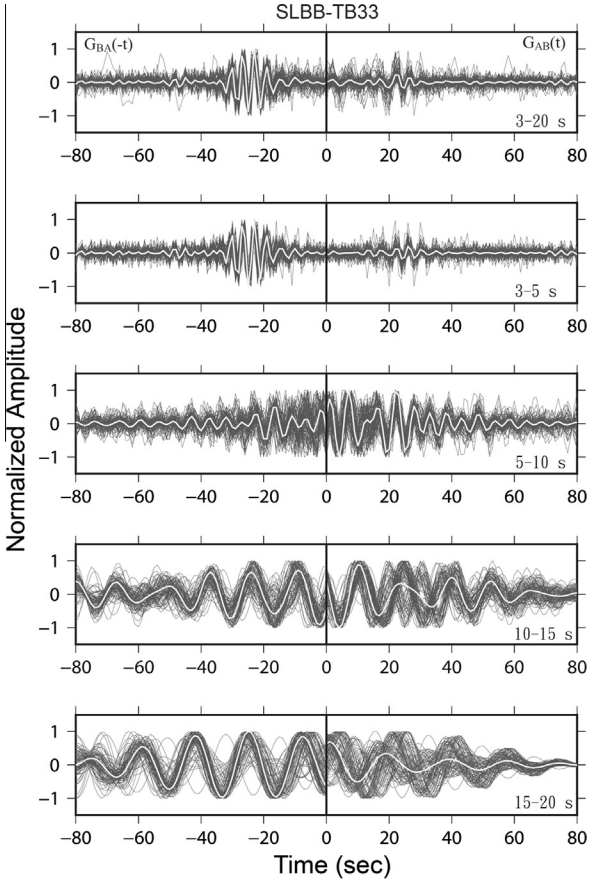

Fig. 3. The daily EGFs (black lines) for three month and the aEGF (white line) stacked from the daily EGFs at various period bands, shown at the lower right of each plot.

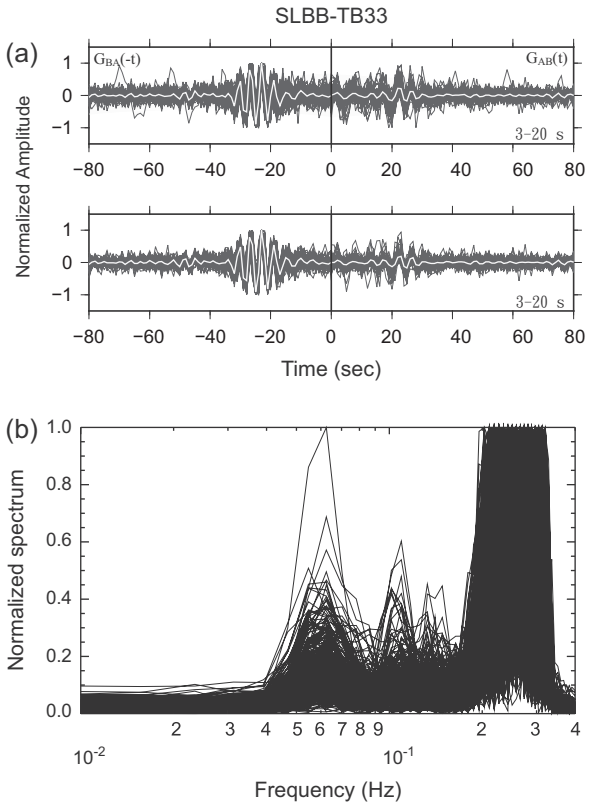

Fig. 4. (a) The top panel indicates the daily EGFs of station SLBB-TB33 for three month and the corresponding aEGF (white line). The bottom panel shows the coherent daily EGFs, which denote cross-correlation coefficients greater than 0.5, compared with the aEGF. A renew aEGF (white line) is presented in the bottom panel. These EGFs are also filtered for periods of 3–20 s. (b) Normalized spectra of the aEGFs, most of which are characterized by periods of 3–6 s.

Herrmann, 1973). In a time–frequency analysis, short-period Rayleigh waves primarily dominated the energy of the EGF, particularly for periods shorter than 7 s. Fig. 5b shows 280 Rayleigh-wave group velocity dispersion curves for periods ranging from 3 to 6 s. Large variations in velocity from about 1.0 to 2.4 km/s at 3 s and from 1.5 to 3.4 km/s at 6 s were observed.

To conveniently explore the velocity variation, we divided the study region into the following seven subregions according to geological features: (1) Tatun Volcano Group, (2) Taipei Basin, (3) Western Coastal Plain, (4) Western Foothills, (5) Hsueshan Range, (6) Ilan Plain, and (7) Central Range (Fig. 5a). Here the subregion (3) was regarded as part of the Western Coastal Plain, the Quaternary cover in Western Taiwan, including the coastal plain, tablelands, and terraces (Ho, 1982, 1986).

The group velocity was determined for each subregion by using the pure-path method (Hwang et al., 2003; Chang et al., 2007). Based on the assumption that surface waves travel along the great-circle path between two stations, the travel time of the path is the sum of the delay time of propagating across each subregions. The travel time from the corresponding group velocity for a given interstation path can be written as follows.

$$t_i(T) = \frac{L_i}{U_{oi}(T)} = \sum_{j=1}^{n} \frac{L_{ij}}{U_j(T)} \quad (2)$$

where $t_i(T)$ is the travel time at period T; L_i is the distance of the ith path; L_{ij} is the partial length of the ith path traveling across the jth subregion. $U_{oi}(T)$ is the observed group velocity for the ith path; $U_j(T)$ is the regionalized group velocity of the jth subregion. Combination of 280 inter-station paths, we transformed the data into the

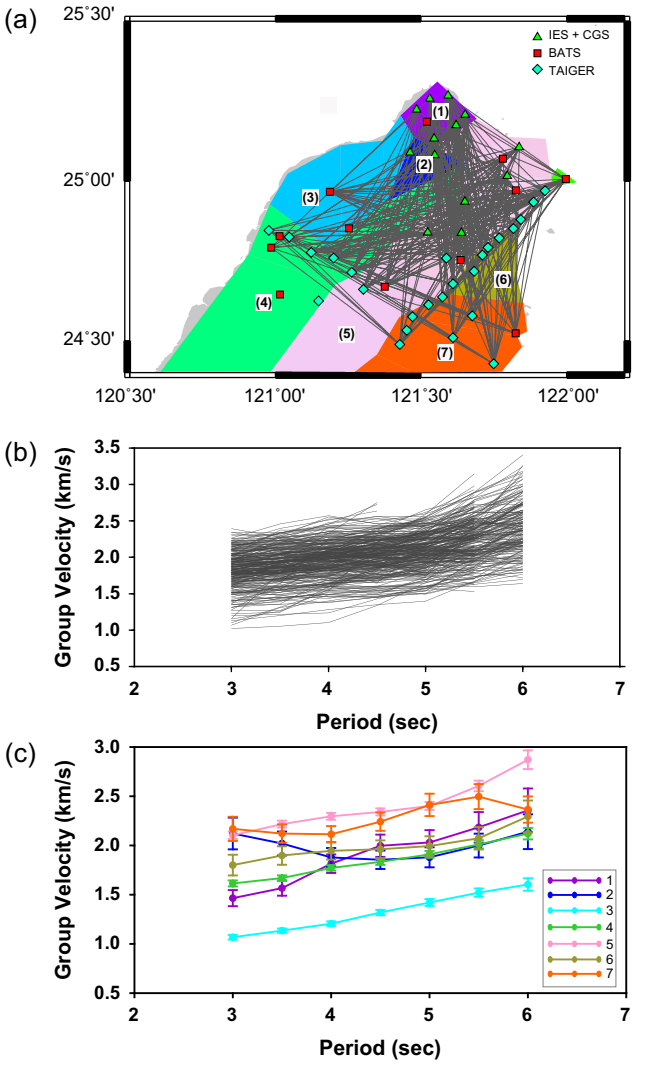

Fig. 5. (a) Distributions of the interstation ray paths. The study region was divided into seven subregions according to the geologic features in Northern Taiwan shown in Fig. 1. (b) The Rayleigh-wave group velocities for periods of 3–6 s for available interstation ray paths. (c) Regionalized Rayleigh-wave group velocities for the seven subregions.

standard linear inversion form, $Ax = b$. A is the kernel matrix, composed of the propagating length across seven subregions; b is the observation vector of group-delay time in this study. x, slowness vector $\lfloor 1/U_j(T) \rfloor$, is the unknown parameter to be inverted using a standard least-squares method (cf. Menke, 1989).

Fig. 5c shows that the regionalized group velocity curves for the seven subregions exhibited obvious velocity variations, which were deeply controlled by the geological characteristics. The regions covered by thick sediment showed a low velocity, whereas the mountain areas indicated a relatively high velocity, consistent with the results of You et al. (2010) and Huang et al. (2012). Among these dispersion curves, the dispersion curve for the Western Coastal Plain exhibited the lowest group velocities, ranging from 1.2 km/s at 3 s to 1.6 km/s at 6 s. This result corresponded to soft sediment and was comparable to the results of Hwang et al. (2003) obtained in Southwestern Taiwan. Similar to the Western Coastal Plain, the averaged curve for the Western Foothills showed smooth pattern, but is about 0.5 km/s higher over the studied period band. On the contrary, the dispersion curves for the Hsueshan Range and Central Range, composed of metamorphic rock, exhibited relatively higher velocities from approximately 2.2 km/s at

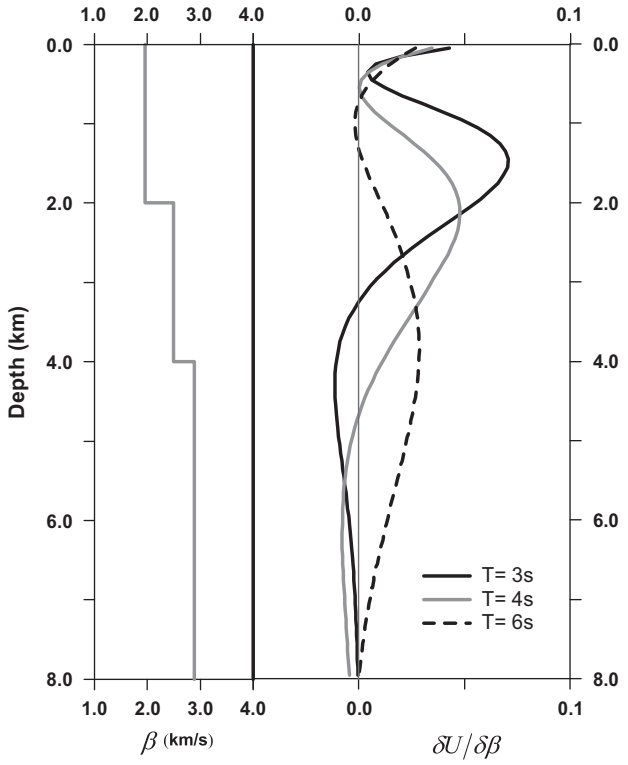

Fig. 6. Sensitivity functions of the fundamental mode Rayleigh-wave group velocity to *S*-wave velocity down to a depth of 6 km, derived from the 1-D *S*-wave velocity model of Chen (1995).

3 s to 2.4 km/s at 5 s. The Hsueshan Range curve rapidly increased at period 5 s, might suggesting the model velocity is high at the deeper part. Moreover, the curve for the Central Range showed a complex pattern that had lower value at 4 s, indicating the structure beneath the Central Range had larger velocity variation with depth. The remaining dispersion curves had velocities between the group velocities of the Western Coastal Plain and those of the Central Range. It is noticeable that the regionalized group velocities of the Taipei Basin showed an Airy phase at 4.5 s, and furthermore the velocities of the Tatun Volcano showed a rapid increase at periods between 3.5 and 4.5 s. Overall, the group velocities increased rapidly from the plain area to the mountain area and were comparable with the tomographic results of Huang et al. (2012).

3.3. S-wave velocity structures

It is well known that the surface waves are mainly handled by the *S*-wave relative to the *P*-wave and density. Therefore, only the *S*-wave velocity is derived in the inversion process by fixing the Poisson's ratio as follows (cf. Hwang and Yu, 2005).

$$\Delta U(T_j) = \sum_{i=1}^{N} \left(\frac{\partial U(T_j)}{\partial \beta_i} \right) \Delta \beta_i \tag{3}$$

where $\Delta U(T_j)$ is the difference between the observed and predicted group velocity at the *j*th period; $\Delta \beta_i$ is the difference in the *S*-wave velocity of the *i*th layer between adjacent inversions; *N* is the number of layers; and $\frac{\partial U(T_j)}{\partial \beta_i}$ is the partial derivative of the *j*th period group velocity with respect to the *S*-wave velocity of the *i*th layer. We adopted a damped least-squares inversion program developed

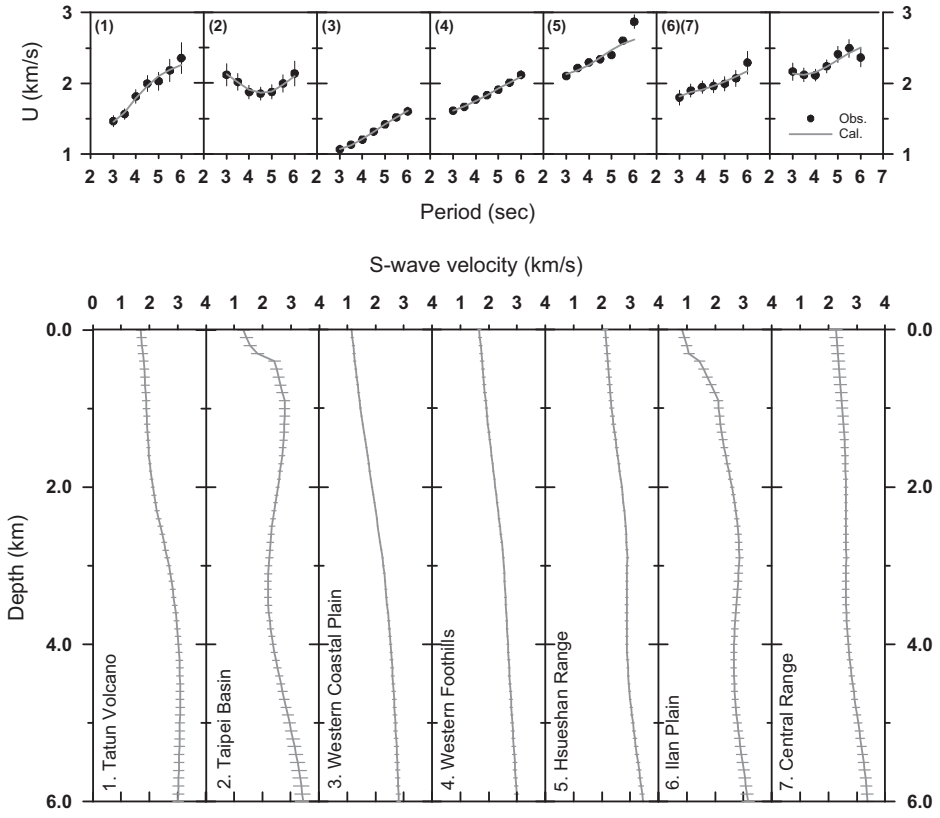

Fig. 7. (Upper) The observed (close circles) and theoretical (lines) group velocities. (Lower) The inverted *S*-wave velocity models down to depths of 6 km for the seven subregions. The standard deviation of velocity is marked by a horizontal bar.

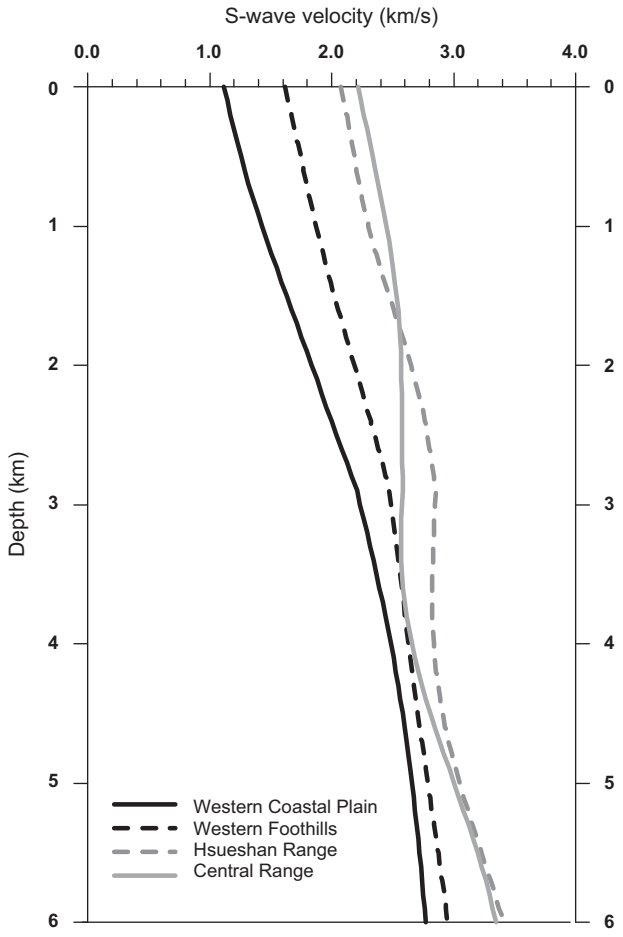

Fig. 8. Comparisons of *S*-wave velocity models for the Western Coastal Plain, Western Foothills, Hsueshan Range, and Central Range.

by Herrmann (1991), and used a smoothing factor to constrain the deviation between adjacent layers during the inversion. Hence, the cost function, , was minimized to perform the inversion of Eq. (3) (cf. Menke, 1989).

$$\Phi = |Ax - b|^2 + \lambda^2 x^T W^T W x \tag{4}$$

where A denotes $\frac{\partial U(T_j)}{\partial \beta_i}$ and b is $\Delta U(T_j)$ as in Eq. (3); x represents the $\Delta\beta_i$ to be inverted; W is the smoothing factor, which provides an approximation of the first-order derivative between adjacent layers; and λ^2 is the damping factor.

We inversed the *S*-wave velocity model for each subregion by the regionalized group velocity for period between 3 and 6 s. A one-dimensional velocity model of Chen (1995) was taken as the initial model in the inversion and the initial model was divided into numerous thin layers, with each layer having a thickness of 0.1 km. The sensitivity functions with periods, derived from the model of Chen (1995), indicated 3–6 s Rayleigh-wave group velocities that were controlled by shallow structures down to 6 km in depth (Fig. 6). During the structure inversion, we put the high Poisson's ratio in the shallow depth of the initial model for the basin areas. The high Poisson's ratio given in the inversion was based on the previous studies of the Taipei Basin (Wang et al., 2004) and the Ilan Plain (Huang, 2003). Fig. 7 shows the seven 1-D *S*-wave velocity structures inverted from their corresponding regionalized group velocities.

4. Discussion

The inverted 1-D *S*-wave models revealed distinguishing characteristics that varied according to the geological unit (Fig. 7). The models of the Western Coastal Plain, Western Foothills, Central Range, and Hsueshan Range illustrated a remarkable lateral variation, indicating that *S*-wave velocities increase from west to east over the entire depth, also in agreement with the *P*-wave tomography (cf. Kim et al., 2005; Wu et al., 2007b; Kuo-Chen et al., 2012). However, the velocities below a depth of 3 km exhibited smaller differences relative to velocities of the top 3 km among these models (Fig. 8). Such a variation is related to the thickness of soft sediment, which decreases from west to east, particularly at a shallow depth above 3 km. Shallow structures, particularly in the *S*-wave velocity model, substantially affect seismic waveforms. In Northern Taiwan, several local *S*-wave structures have been estimated by microtremors (Li, 2007; Kuo et al., 2009) and short-period surface waves (Chung and Shin, 1999; Huang, 2003). However, this study is the first to obtain the shallow *S*-wave structures of the individual geological units in Northern Taiwan. The shallow structures inverted from the 3–6 s group velocity curves had lower resolution near the surface than those by using high-frequency microtremor analysis, but providing more in-depth information in Northern Taiwan. Moreover, the regionalized model illustrated the common characteristics of the specific geological units.

Because of the thick layer of unconsolidated sediment, the subsurface velocities in the Western Coastal Plain were low, whereas the Central and Hsueshan Ranges exhibited high *S*-wave velocities attributable to metamorphic rock. The gradients of the *S*-wave velocity (approximately 0.3 km/s per km) captured in the Hsueshan Range and the Western Foothills were similar, but the velocities for the Hsueshan Range were much higher (Fig. 8). We compared our results with those of previous studies. Fig. 9a shows that, on average, the derived model of the Western Foothills is similar to the 1-D average model of Chen (1995), as mentioned by Hwang et al. (2003). To identify the difference of the Western Coastal Plain, we compared the models obtained by Hwang et al. (2003) in Southwestern Taiwan. They divided the south Western Coastal Plain into two regions from east to west, regarded as Region 2 and Region 3, resulting from the obvious difference. The *S*-wave velocity of the Western Coastal Plain obtained in this study is consistent with that of Region 2, but is higher than that of Region 3, in the work of Hwang et al. (2003) (Fig. 9b). This is because Region 3 in Hwang et al. (2003) was near the coast, where the recent sediment is thicker. The 1-D *P*-wave model of the Tatun Volcano Group was derived by Lin and Yeh (1989, personal communication), and the corresponding *S*-wave model was obtained by applying the constant V_p/V_s ratio, 1.78, where V_p is the *P*-wave velocity and V_s is the *S*-wave velocity (Lin et al., 2005). The 1-D model of both the *P*- and *S*-waves was employed to locate microevents in the Tatun volcanic area. Fig. 9c shows a comparison of the *S*-wave velocity model constructed in this study and the model of the Tatun Volcano Group used by Lin et al. (2005). At the top 3 km, the *S*-wave velocity inverted by this study lower than that applied by Lin et al. (2005) was to suggest that the V_p/V_s value should be high at a shallow depth in the Tatun volcanic area. This was comparable to the observations of the area beneath volcanoes in northeastern Japan (Nakajima et al., 2001).

Excluding the Taipei Basin and the Ilan Plain, the other regions displayed uniform variations in the velocity gradient over the entire depths. In the top 1 km of the model, the Taipei Basin and the Ilan Plain had a larger velocity gradient. Generally, the velocity gradient at the top 3 km of these models decreased from west with 0.39 km/s per km to east with 0.15 km/s per km.

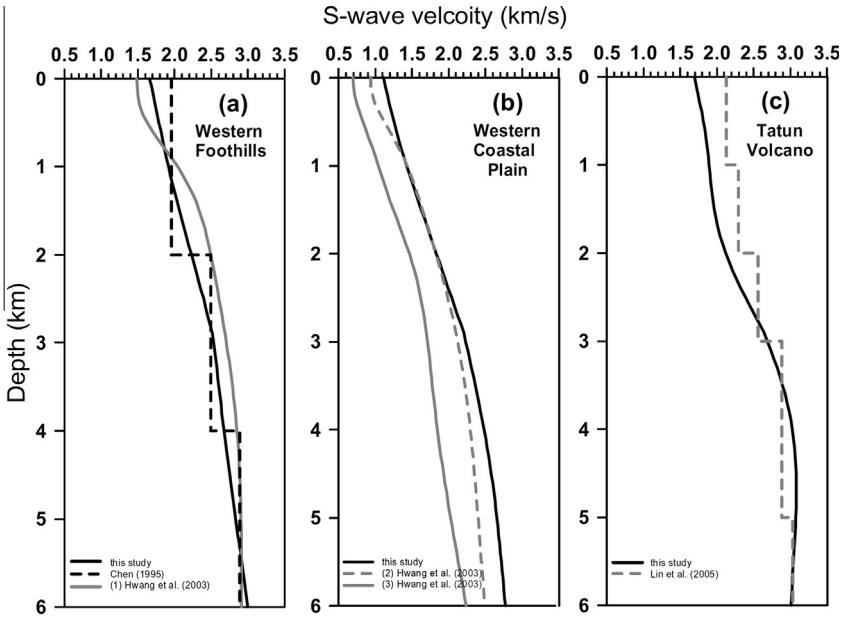

Fig. 9. Comparisons between our models and those of previous studies (Chen, 1995; Hwang et al., 2003; Lin et al., 2005) for (a) Western Foothills, (b) Western Coastal Plain, and (c) Tatun Volcano Group.

Among these models, the Western Coastal Plain showed a higher *S*-wave velocity gradient, 0.39 km/s per km. Huang et al. (2013) observed a high *P*-wave velocity gradient of approximately 0.72 km/s per km in the Western Coastal Plain from an analysis of multiple diving waves along a SE-NW linear array deployed in south Taiwan. Following $V_P = \sqrt{3}V_S$ and Huang et al. (2013), we calculated the corresponding *S*-wave velocity gradient of 0.42 km/s per km, which is comparable with the results obtained in this study. The *S*-wave models of southwestern Taiwan derived by Hwang et al. (2003) also showed a high velocity gradient, with an average of 0.40 km/s per km in the Western Coastal Plain. As mentioned above, this implies that the *S*-wave velocity gradient in the Western Coastal Plain from north to south is consistently high in the Taiwan region. Our models can facilitate further analysis of the diving *S*-wave simulation as the estimation of the *P*-wave (Huang et al., 2013).

The Taipei Basin and the Ilan Plain exhibited higher velocity gradients than other regions did. This indicates that seismic waves were likely to be trapped at a shallow depth and become amplified (Fig. 7). This would be a remarkable fact for those regions when a large earthquake occurs as observed in the 1995 Hyogo-ken Nanbu earthquake (Kawase et al., 2000). Wang et al. (2000) studied the effects of the velocity gradient on the waveform amplification, and showed lower surface-wave velocity, longer duration, and larger amplitude on ground motions when increasing the velocity gradient of the model. In contrast to the Western Foothills, the seismograms recorded in the Western Coastal Plain showed longer period signals (Hwang et al., 2003). Such short-period surface waves were easy to induce, because the waves were trapped within the layers with a high velocity gradient. Generally, a long duration of ground shaking may cause greater damage than a short duration of motion does. That is, low velocity was a crucial factor to make seismic waves amplified (Hwang et al., 2003; Lee et al., 2007). Using waveform simulation, Lee et al. (2007) observed that the shallow low-velocity layer of the Western Coastal Plain significantly amplified ground motions. The detailed shallow-depth velocity structures, combined with the near-surface structure determined by using microtremor analysis (Wu and Huang, 2013), can be used to predict ground motion and, thus, assess seismic hazards.

5. Conclusion

The Rayleigh-wave group velocities in Northern Taiwan, analyzed according to ambient noise, exhibited obvious lateral variations. From the regionalized group velocities at periods from 3 to 6 s, the coastal plain area showed low group velocities caused by thick and soft sediments, whereas the mountain areas displayed high group velocities attributable to metamorphic rocks. The corresponding inverted *S*-wave velocity models also indicated clear lateral variation. From west to east, the *S*-wave velocities increased significantly down to 6-km depths. At shallow depths, the Taipei Basin and the Ilan Plain with high velocity gradients caused seismic waves to be amplified more easily than they are in other regions. At the top 3 km of the velocity model, the velocity gradient (approximately 0.39 km/s per km) of the Western Coastal Plain was higher than that of the mountainous areas, consistent with previous results obtained in Southwestern Taiwan. The *S*-wave models derived in this study according to geological features can provide strong constraints on predicting ground motion and, thus, facilitate seismic hazard assessment.

Acknowledgments

This study was supported by the Central Geology Survey and the Ministry of Science and Technology of Taiwan under grants MOST 103-211-M-001-022 and MOST 103-2116-M-001-023. We thank the Central Geology Survey and the Institute of Earth Science, Academia Sinica, for the data and logistical support. We also thank the two anonymous reviewers for their critical suggestions for improving the manuscript.

References

Bensen, G.D., Ritzwoller, M.H., Barmin, M.P., Levshin, A.L., Lin, F., Moschetti, M.P., Shapiro, N.P., Yang, Y., 2007. Processing seismic ambient noise data to obtain reliable broad-band surface wave dispersion measurements. Geophys. J. Int. 169, 1239–1260. http://dx.doi.org/10.1111/j.1365-246X.2007.03374.x.

Bromirski, P.D., Duennebier, F.K., Stephen, R.A., 2005. Mid-ocean microseisms. Geochem. Geophys. Geosyst. 6. http://dx.doi.org/10.1029/2004GC000768.

Campillo, M., Paul, A., 2003. Long-range correlations in the diffuse seismic coda. Science 299, 547–549.

Chang, W.Y., Yu, G.K., Hwang, R.D., Chiu, J.K., 2007. Lateral variations of Rayleigh wave dispersions in the Philippine Sea region. Terr., Atmos. Oceanic Sci. 18, 859–878. http://dx.doi.org/10.3319/TAO.2007.18.5.859(T).

Chen, Y.L., 1995. Three Dimensional Velocity Structure and Kinematic Analysis in Taiwan area, M.S. thesis, Inst. of Geophys., Natl. Cent. Univ., Chung-Li, Taiwan. (in Chinese with English abstract).

Chen, Y.N., Gung, Y., You, S.H., Hung, S.H., Chiao, L.Y., Huang, T.Y., Chen, Y.L., Liang, W.T., Jan, S., 2011. Characteristics of short period secondary microseisms (SPSM) in Taiwan: the influence of shallow ocean strait on SPSM. Geophys. Res. Lett. 38, L04305. http://dx.doi.org/10.1029/2010GL046290.

Chung, J.K., Shin, T.C., 1999. Surface-wave analysis in the Taipei basin from strong-motion data. Terr., Atmos. Oceanic Sci. 10, 633–650.

Derode, A., Tourin, A., Fink, M., 1999. Ultrasonic pulse compression with one-bit time reversal through multiple scattering. J. Appl. Phys. 85, 6343–6352.

Dziewonski, A., Bloch, S., Landisman, M., 1969. A technique for the analysis of transient seismic signals. Bull. Seismol. Soc. Am. 59, 427–444.

Herrmann, R.B., 1973. Some aspects of band-pass filtering of surface waves. Bull. Seismol. Soc. Am. 63, 703–711.

Herrmann, R.B., 1991. Computer programs in seismology, vol. IV. Surface Wave Inversion. Dep. of Earth and Atmos. Sci., Saint Louis Univ., Saint Louis, Mo.

Ho, C.S., 1982. Tectonic Evolution of Taiwan: Explanatory Text of the Tectonic Map of Taiwan. Central Geology Survey, Ministry of Economic Affairs, Taiwan.

Ho, C.S., 1986. A synthesis of the geologic evolution of Taiwan. Tectonophysics 125, 1–16.

Huang, Y.C., 2003. Site Effect and Near Surface S Wave Velocity Structure in Lan-Yang Plain, M.S. thesis, Inst. of Geophys., Natl. Cent. Univ., Chung-Li, Taiwan. (in Chinese with English abstract).

Huang, H.C., Wu, C.F., 2006. Estimations of the S-wave velocity structures in Chia-Yi City, Taiwan, using the array records of microtremors. Earth, Planets and Space 58, 1455–1462.

Huang, Y.C., Yao, H., Huang, B.S., van der Hilst, R.D., Wen, K.L., Huang, W.G., Chen, C.H., 2010. Phase velocity variation at periods of 0.5–3 seconds in the Taipei basin of Taiwan from correlation of ambient seismic noise. Bull. Seismol. Soc. Am. 100, 2250–2263. http://dx.doi.org/10.1785/0120090319.

Huang, T.Y., Gung, Y., Liang, W.T., Chiao, L.Y., Teng, L.S., 2012. Broad-band Rayleigh wave tomography of Taiwan and its implication on gravity anomalies. Geophys. Res. Lett. 39, L05305. http://dx.doi.org/10.1029/2011GL050727.

Huang, B.S., Wang, C.Y., Okaya, D., Lee, S.-J., Lai, Y.C., Wu, F.T., Liang, W.T., Huang, W.G., 2013. Multiple diving waves and steep velocity gradients in the western Taiwan coastal plain: an investigation based on the TAIGER experiment. Bull. Seismol. Soc. Am. 103, 925–935. http://dx.doi.org/10.1785/0120110047.

Hwang, R.D., Yu, G.K., 2005. Shear-wave velocity structure of upper mantle under Taiwan from the array analysis of surface waves. Geophys. Res. Lett. 32, L07310. http://dx.doi.org/10.1029/2004GL021868.

Hwang, R.D., Yu, G.K., Chang, W.Y., Chang, J.P., 2003. Lateral variations of shallow shear-velocity structure in southwestern Taiwan inferred from short-period Rayleigh waves. Earth, Planets and Space 55, 349–354.

Kawase, H., Matsushima, S., Graves, R.W., Somerville, P.G., 2000. Strong motion simulation of Hyogo-ken Nanbu (Kobe) earthquake considering both the heterogeneous rupture process and the 3D basin structure. Proceedings of the 12th World Conference on Earthquake Engineering, Auckland, New Zealand, CD-ROM Ref. No. 990.

Kim, K.H., Chiu, J.M., Pujol, J., Chen, K.C., Huang, B.S., Yeh, Y.H., Shen, P., 2005. Three-dimensional Vp and Vs structural model associated with the active subduction and collision tectonics in the Taiwan region. Geophys. J. Int. 162, 204–220.

Kuo, C.H., Cheng, D.S., Hsieh, H.H., Chang, T.M., Chiang, H.J., Lin, C.M., Wen, K.L., 2009. Comparison of three different methods in investigating shallow shear wave velocity structures in Ilan, Taiwan. Soil Dyn. Earthquake Eng. 29, 133–143. http://dx.doi.org/10.1016/j.soildyn.2009.01.010.

Kuo-Chen, H., Wu, F.T., Roecker, S.W., 2012. Three-dimensional P velocity structures of the lithosphere beneath Taiwan from the analysis of TAIGER and related seismic datasets. J. Geophys. Res. 117, B06306. http://dx.doi.org/10.1029/2011JB009108.

Lee, S.J., Chen, H.W., Ma, K.F., 2007. Strong ground motion simulation of the 1999 Chi–Chi, Taiwan earthquake from a realistic three-dimensional source and crustal stricture. J. Geophys. Res. 112, B06307. http://dx.doi.org/10.1029/2006JB004615.

Li, F.M., 2007. Shallow S-Wave Velocity Structures of the Taipei Basin, Taiwan, Estimated from Array Records of Microtremors, M.S. thesis, Inst. of Seismo., Natl. Chung Cheng Univ., Taiwan. (in Chinese with English abstract).

Lin, C.H., Konstantinou, K.I., Pu, H.C., Hsu, C.C., Lin, Y.M., You, S.H., Huang, Y.P., 2005. Preliminary results of seismic monitoring at Tatun volcanic area of northern Taiwan. Terr., Atmos. Oceanic Sci. 16, 563–577.

Lin, C.M., Chang, T.M., Huang, Y.C., Chiang, H.J., Kuo, C.H., Wen, K.L., 2009. Shallow S-wave velocity structures in the western coastal plain of Taiwan. Terr., Atmos. Oceanic Sci. 20, 299–308. http://dx.doi.org/10.3319/TAO.2007.12.10.01(T).

Lobkis, O.I., Weaver, R.L., 2001. On the emergence of the Green's function in the correlations of a diffusive field. J. Acoust. Soc. Am. 110, 3011–3017.

Menke, W., 1989. Geophysical Data Analysis: Discrete Inversion Theory. Academic Press, London, 289 pp.

Nakajima, J., Matsuzawa, T., Hasegawa, A., Zhao, D., 2001. Three-dimensional structure of Vp, Vs, and Vp/Vs beneath northeastern Japan: implications for arc magmatism and fluids. J. Geophys. Res. 106, 21843–21857.

Okaya, D., Wu, F.T., Wang, C.Y., Yen, H.Y., Huang, B.S., Brown, L., Liang, W.T., 2009. Joint passive/controlled source seismic experiment across Taiwan. EOS Trans. AGU 90, 289–290.

Sabra, K.G., Gerstoft, P., Roux, P., Kuperman, W.A., 2005. Surface wave tomography from microseisms in Southern California. Geophys. Res. Lett. 32, L14311. http://dx.doi.org/10.1029/2005GL023155.

Satoh, T., Kawase, H., Iwata, T., Higashi, S., Sato, T., Irikura, K., Huang, H.C., 2001. S-wave velocity structure of the Taichung basin, Taiwan, estimated from array and single-station records of microtremors. Bull. Seismol. Soc. Am. 91, 1267–1282.

Shapiro, N.M., Campillo, M., 2004. Emergence of broadband Rayleigh waves from correlations of the ambient seismic noise. Geophys. Res. Lett. 31, L07614. http://dx.doi.org/10.1029/2004GL019491.

Shapiro, N.M., Campillo, M., Stehly, L., Ritzwoller, M.H., 2005. High-resolution surface wave tomography from ambient seismic noise. Science 307, 1615–1618.

Tsai, Y.B., 1986. Seismotectonics of Taiwan. Tectonophysics 125, 17–37.

Wang, C.Y., Shin, T.C., 1998. Illustrating 100 years of Taiwan seismicity. Terr., Atmos. Oceanic Sci. 9, 589–614.

Wang, Y., Takenaka, H., Furumura, T., 2000. Effect of vertical velocity gradient on ground motion in a sediment-filled basin due to incident SV wave. Earth Planets Space 52, 13–24.

Wang, C.Y., Lee, Y.-H., Ger, M.L., Chen, Y.-L., 2004. Investigating subsurface structures and P- and S-wave velocities in the Taipei basin. Terr., Atmos. Oceanic Sci. 15, 609–627.

Wu, C.F., Huang, H.C., 2013. Near-surface shear-wave velocity structure of the Chiayi area, Taiwan. Bull. Seismol. Soc. Am. 103, 154–1164. http://dx.doi.org/10.1785/0120110242.

Wu, F.T., Lavier, L.L.TAIGER Teams, 2007a. Collision tectonics of Taiwan and TAIGER experiments. EOS Trans. AGU 88 (52) (Fall Meet. Suppl.), T51A-0321.

Wu, Y.M., Chang, C.H., Zhao, L., Shyu, J.B.H., Chen, Y.G., Sieh, K., Avouac, J.P., 2007b. Seismic tomography of Taiwan: improved constraints from a dense network of strong-motion stations. J. Geophys. Res. 112, B08312. http://dx.doi.org/10.1029/2007JB004983.

Wu, F.T., Kuo-Chen, H., McIntosh, K.D., 2014. Subsurface imaging, TAIGER experiments and tectonic models of Taiwan. J. Asian Earth Sci. 90, 173–208. http://dx.doi.org/10.1016/j.jseaes.2014.03.024.

Yao, H., van der Hilst, R.D., de Hoop, M.V., 2006. Surface-wave array tomography in SE Tibet from ambient seismic noise and two-station analysis: I – phase velocity maps. Geophys. J. Int. 166, 732–744.

You, S.H., Gung, Y., Chiao, L.Y., Chen, Y.N., Lin, C.H., Liang, W.T., Chen, Y.L., 2010. Multiscale ambient noise tomography of short-period Rayleigh waves across northern Taiwan. Bull. Seismol. Soc. Am. 100, 3165–3173. http://dx.doi.org/10.1785/0120090394.